Evidence for the importance of growth-surface structure to trace element incorporation in topaz

Paul A. Northrup, Richard J. Reeder

Department of Earth and Space Sciences, State University of New York at Stony Brook,
Stony Brook, New York 11794-2100, U.S.A.

Abstract

Trace element distributions in topaz [$Al_2SiO_4(F,OH)_2$] single crystals display both sectoral and intrasectoral zoning of trace elements as a function of growth-surface structure. Differential interference contrast microscopy shows that the dominant {110} form exhibits large, polygonized, spiral growth hillocks with four vicinal faces, each comprising an array of parallel growth steps. Cathodoluminescence microscopy and synchrotron X-ray fluorescence microanalysis show that during growth trace elements (As, Fe, and Ti) were differentially incorporated into vicinal faces having symmetrically nonequivalent step orientations, producing intrasectoral zoning in the bulk crystal. Subsectors that formed from vicinal faces related by surface symmetry possess identical compositions. In all cases, there is precise correlation between surface microtopography and trace element distribution, demonstrating a surface-structural control of trace element incorporation. Concentrations of As in time-equivalent regions of different subsectors within the {110} growth sector differ by as much as 9:1. Ti and Fe also differ significantly. Similar intrasectoral zoning related to surface-growth step orientation occurs on spiral growth hillocks on the {010}, {001}, and {111} forms as well.

Sectoral zoning is also present in the majority of samples examined. Differences in trace element concentrations between time-equivalent regions of symmetrically nonequivalent growth sectors are large, up to 100:1 for As and between 23:1 and 7:5 for Fe, Ti, Ga, Ge, and Nb.

Trace elements proxy for major elements in the structure but possess differences that significantly affect their incorporation at the surface. Zoning patterns preserve a record of that effect. Arrays of growth steps migrating in nonequivalent directions on a given surface, as well as growth surfaces of nonequivalent crystal forms, differ in their detailed structure of incorporation sites and can differentially incorporate trace elements into coeval regions within a single crystal. Therefore, no single value of the distribution coefficient of a trace element can be applied for all areas of the crystal surface during growth. This indicates that the value of the distribution coefficient is path-dependent and thus not governed by equilibrium. Moreover, nonequivalent growth step orientations exhibit differences in such kinetic properties as step spreading (growth) rate and degree of curvature.

Introduction

The use of trace elements in many geochemical investigations is predicated on the knowledge of their distribution behavior. Such work, however, has rarely considered the surface-structural dependence of trace element incorporation. At thermodynamic equilibrium under given conditions of pressure, temperature, and bulk composition, the concentration of a trace element in a solid relative to that in a coexisting fluid is a fixed value, traditionally defined as the distribution coefficient (D). However, surface orientation and microtopography are observed to influence the incorporation of trace elements into different areas of a crystal surface during growth. This is demonstrated in many minerals by sectoral and intrasectoral zoning, which are expressed as compositional differences between time-equivalent growth regions of a single crystal. These phenomena suggest that a surface-specific factor causes variation in the actual D. This surface-induced segregation is then inherited by the bulk crystal as growth proceeds.

Sectoral zoning (e.g., Nakamura, 1973; Dowty, 1976) is the simultaneous formation, by growth on nonequivalent crystal faces, of compositionally different regions (sectors). Despite being a relatively well-known phenomenon, sectoral zoning still presents questions as to the specific mechanism for differential incorporation. Only recently recognized, intrasectoral zoning (e.g., Paquette
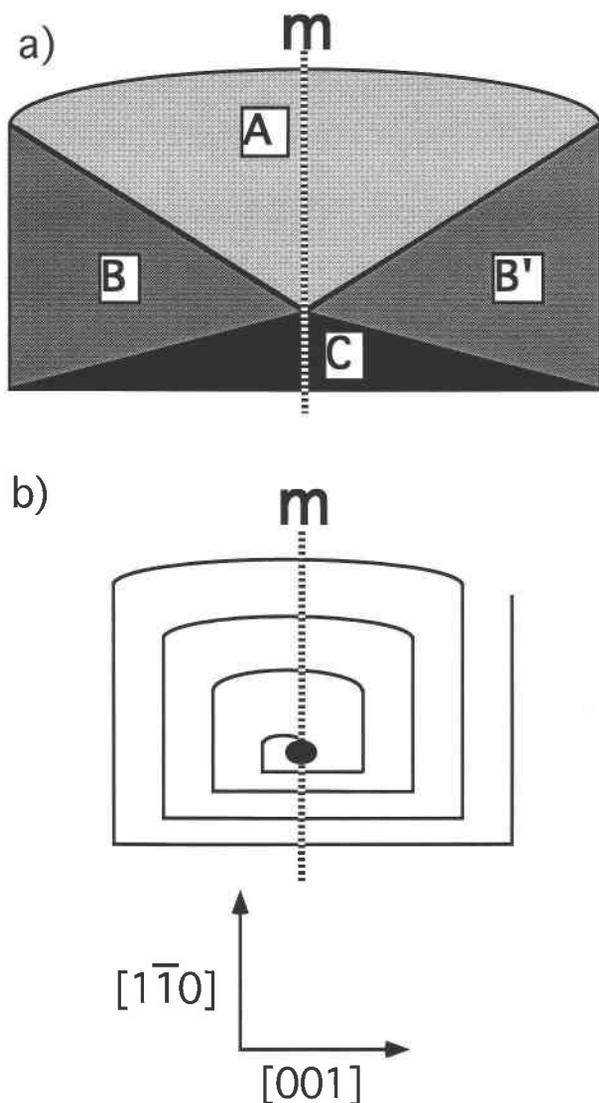
Fig. 1. (a) Schematic plan view of a polygonized spiral-growth hillock as observed on topaz (110). Vicinal faces A, B, B', and C are labeled as such throughout this paper. (b) A surface imperfection, such as an emerging screw dislocation (solid circle), produces a perpetual step forming a growth spiral. Preferential orientation of growth steps parallel to [1$\bar{1}$0] and [001] results in polygonization. Steps on B and B' are related by a mirror (m).

poration of both major and trace elements is believed to occur at these kink sites. From this more detailed perspective, differences in the three-dimensional structure of surface kink sites may explain both sectoral and intrasectoral zoning.

Intrasectoral zoning is best shown by surfaces exhibiting polygonized spiral-growth hillocks. Growth on a flat (F) form (Hartman and Perdok, 1955) often occurs by the spiral mechanism (Fig. 1). The emergence of a screw dislocation at the crystal surface allows for the existence of a perpetual step. Since growth occurs mostly at kink sites along steps, a growth spiral is formed, centered around the dislocation. Steps migrate out from the dislocation and form a low mound (a growth hillock). Steps may become aligned along directions of repeated strong bonds. In that case, the hillock becomes polygonized with distinct shallow planar flanks called vicinal faces.

Because each vicinal face of a growth hillock consists of an array of parallel, structurally similar growth steps, the particular region of the crystal grown as that vicinal face advances is defined as a growth subsector. It may be treated in the same way as face-specific growth sectors. Step orientations on vicinal faces related by appropriate surface symmetry operators must have identical structures and properties. Their corresponding subsectors are expected to have the same composition. Symmetrically nonequivalent step orientations, however, differ in their detailed structure and have the potential for differentially incorporating trace elements. Ideally, all hillocks on all equivalent faces of a given crystal must have exactly equivalent morphology, vicinal face slopes, and trace element distribution patterns.

This work characterizes trace element incorporation in topaz and correlates zoning patterns with differences in surface microtopography. The purpose of this study is to test, apply, and extend our understanding of differential incorporation processes originally developed for calcite grown in solution. Previously, intrasectoral zoning had only been documented in calcite (Paquette and Reeder, 1990) and diamond (Frank et al., 1990). To our knowledge, topaz is the first silicate shown to possess intrasectoral, as well as sectoral, zoning of trace elements (Northrup and Reeder, 1992). Several characteristics make topaz especially well suited for the study of surface-dependent processes. It commonly grows by the spiral mechanism on several forms; it is mechanically and chemically resistant and preserves natural microtopography; and it has sufficiently complex crystal chemistry to provide useful information about trace element incorporation.

SAMPLES AND EXPERIMENTAL METHODS

This study focuses on near F end-member topaz ($Al_2SiO_4F_2$) crystals from near Tepetates, San Luis Potosí, Mexico. They occur in lithophysae in rhyolite lava flows and domes that are 7–30 m.y. old. The deposits are similar to those in the Thomas Mountains of Utah, in which topaz is believed to have crystallized from a high-

and Reeder, 1990; Reeder, 1991a, 1991b) results from the differential incorporation of trace elements into time-equivalent regions of a single growth sector. Both sectoral and intrasectoral zoning have well-defined and systematic spatial arrangements within a single crystal and result solely from growth processes (Reeder, 1991b). The results of studies of intrasectoral zoning in calcite (Paquette and Reeder, 1990; Staudt et al., 1994) suggest that the key factor for differential incorporation is the different coordination geometry of kink sites within growth steps having different orientations on a crystal surface. The incor-

temperature, low-density vapor phase (Roedder and Stalder, 1988). Trace elements (Ti, Fe, Ga, Ge, As, and Nb) detected by X-ray fluorescence (described below) are present in concentrations below approximately 500 ppm. Large polygonized spiral-growth hillocks occur on {110}, {001}, {010}, and {111}. Whereas sectoral and intrasectoral zoning are both present in these topaz crystals, the emphasis here is placed on intrasectoral zoning, particularly on the {110} form, which is dominant in these crystals and in most other F-rich topaz.

Cathodoluminescence (CL) microscopy was used for the examination of qualitative differences of certain trace elements as they act as CL activators or quenchers. The intensity and sometimes color of luminescence observed are functions of the concentrations, so that compositional differences can be easily mapped. Differential interference contrast (DIC) microscopy allows slight variations in height and inclination (microtopography) of surfaces to be seen as differences in color. This technique was utilized for imaging the vicinal faces of growth hillocks, which may have slopes of only 0.05–2.0° from the crystal face. Vicinal face slopes were measured using the angular divergence of reflected light by a high-resolution method developed for this study.

Because of the low concentration of trace elements, synchrotron X-ray fluorescence microanalysis (SXRFMA), rather than the electron microprobe, was used for compositional analysis. SXRFMA was conducted at beam line X26A of the National Synchrotron Light Source at Brookhaven National Laboratory. Minimum detection limits for most trace elements with atomic weights greater than that of Si are 0.5–10 ppm using a ~10-μm beam. Spatially resolved, relative differences in concentration (e.g., zoning) can be determined with high precision, approximately 0.8% (relative) for point analyses within an experimental session. For absolute concentrations, however, uncertainties may exceed 10%. Concentrations from point analyses, line scans, and area scans were derived using procedures described by Criss (1977) and Lu et al. (1989).

RESULTS

The {110} form

DIC and CL microscopy and characterization by SXRFMA of several {110} surface sections showed consistent patterns among all crystals examined. The (110) surface of sample MX-2 contains a four-sided growth hillock 1.8 × 2 mm and 7 μm high at its apex (Fig. 2a). Vicinal faces B and B′ comprise growth steps aligned parallel to [1$\bar{1}$0] and oriented so as to advance toward −c and +c, respectively. Vicinal faces A and C consist of steps parallel to [001], which advance in opposite directions. Individual growth steps, presumably of monolayer height or a small multiple thereof, cannot be directly observed using DIC. However, macrosteps, assumed to be parallel to individual growth steps, are clearly visible in Figure 2a and on the (110) surface of another crystal (Fig. 3a).
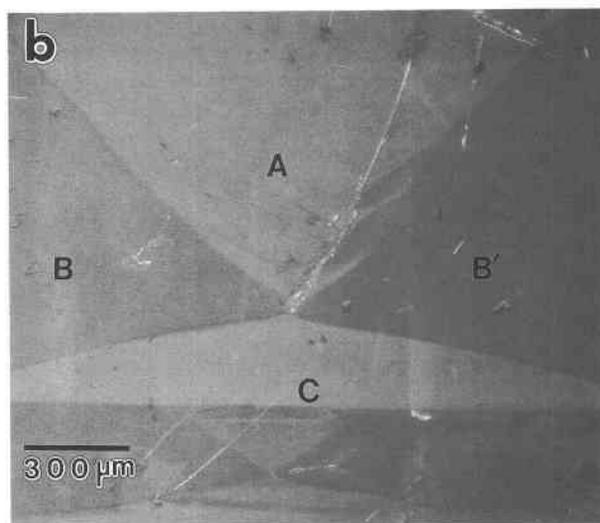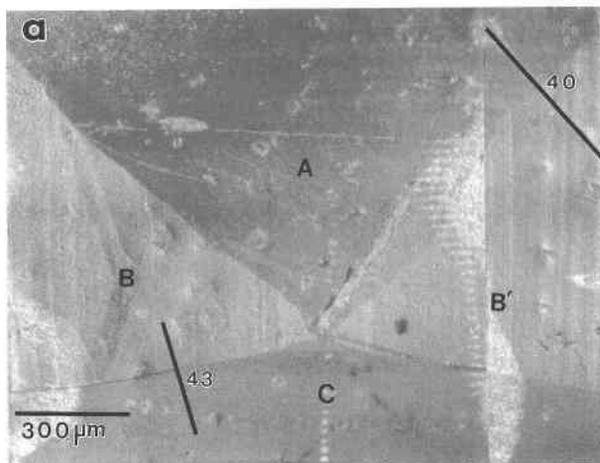
Fig. 2. (a) DIC photomicrograph of a growth hillock on topaz (110). The orientation is the same as in Fig. 1. Four distinct vicinal faces (A, B, B′, and C, as in Fig. 1) are evident. Traverses labeled 40 and 43 show positions of SXRFMA line scans. (b) Corresponding CL photomicrograph (Technosyn model 8200 MK2 cold-cathode Luminoscope operating at 12 kV and 580 μA). Observed luminescence colors are as follows: A represents blue, B and B′ are both the same shade of tan, and C is yellow.

A mirror perpendicular to {110} and to the c axis relates steps advancing toward +c and −c, making the steps on vicinal faces B′ and B structurally equivalent. There is no such relationship between vicinal faces A and C. On the hillock shown in Figure 2, the slopes of the vicinal faces relative to the {110} plane are 0.1° for A, 0.2° for B and B′, and 0.4° for C. Differences in growth characteristics and lateral spreading rates between nonequivalent step orientations are expressed in the asymmetry of the hillock and in the distinct curvature of the steps only seen on vicinal face A.

Corresponding CL photomicrographs (Figs. 2b and 3b) show that, for each face, the luminescence pattern cor-
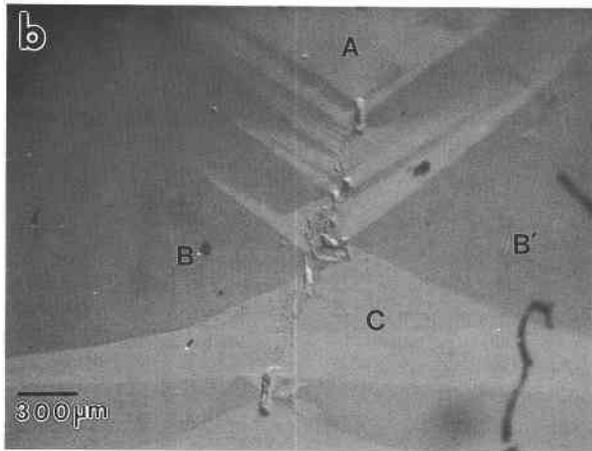
Fig. 3. (a) DIC photomicrograph of a growth hillock on (110) of a second topaz crystal, in the same orientation as Fig. 1. Macrosteps are apparent and show complex growth around an outcropping inclusion. (b) Corresponding CL photomicrograph. Note the strict correspondence of the CL pattern to the complex microtopography and to the mirror symmetry. Observed CL colors are the same as in Fig. 2.

TABLE 1. SXRFMA results of point analyses on a topaz (110) surface section showing intrasectoral zoning

Subsector*	A	B	B'	C
CL color	blue	tan	tan	yellow
Ti (ppm)	256(3)	207(2)	205(2)	153(2)
Fe (ppm)	172(2)	208(2)	206(2)	224(3)
Ga (ppm)	6(1)	7(1)	7(1)	8(1)
Ge (ppm)	24(1)	23(1)	24(1)	22(1)
As (ppm)	5.5(1)	15(1)	16(1)	40(1)

* Location of subsectors shown in Fig. 2 (also see text).

blue, the weaker yellow appears as a shade of tan. Polishing the crystal surface and cutting cross sections confirmed that the zoning pattern on the surface of the hillock is preserved into the interior of the {110} growth sector and crosscuts concentric zones.

The hillock on sample MX-2 (Fig. 2) was prepared as a surface section, 110 μm thick and 2 × 3 mm across. Each surface section for SXRFMA was sliced from the crystal, polished from the back, and mounted on an ultrapure silica-glass slide, with the growth surface exposed. The section consists of a thin slice containing the crystal face, and therefore all analyses of it represent time-equivalent positions. Several point analyses were collected in the subsectors below each vicinal face. The averaged results are summarized in Table 1. Line-scan analyses (points 10 μm apart) were collected across the hillock, from subsector A into B' and from B into C (Fig. 4). As, Fe, and Ti showed discontinuous changes in concentration exactly at vicinal face boundaries. Well-defined differences of 2.5:1 and 7:1 are present for As concentrations. Fe and Ti distributions are somewhat obscured by the presence of minute oxide inclusions but show relative differences of up to 20%. Ti also displays additional variations within the subsectors (discussed below). The observed trace elements do not all follow the same partitioning pattern. Whereas As and Fe are highest in subsector C and lowest in subsector A, Ti is highest in A and lowest in C. Subsectors B and B' are intermediate in all three elements. In contrast, Ga and Ge possess the same concentrations in all subsectors within analytical precision.

Area scans, two-dimensional arrays of point analyses, were also conducted to map zoning patterns and the distribution of inclusions. Compositional contour maps of the hillock clearly delineated the four subsectors exactly as described by CL and the line scans, confirming the spatial distribution of trace elements in accord with the different subsectors (e.g., As, in Fig. 5). Ti again showed irregular variations in concentration within subsectors, but these variations were always smaller than the differences between subsectors. Sharp spikes in the concentrations of Ca, Fe, Ti, Mn, and Nb record the existence and location of inclusions in both line and area scans.

With only minor variations, the described microtopography, CL pattern, and relative trace-element concentrations were found to occur in all crystals examined from

responds exactly to the vicinal faces of the hillock. Because CL is emitted from a finite thickness of material (~5 μm), it reflects the near-surface composition of that subsector. Vicinal face A (and its corresponding subsector) luminesces deep blue. An acquired CL spectrum showed a broad peak centered at approximately 570 nm, and no polarization of the emitted light was evident. This peak is present in the spectra for all subsectors and throughout the bulk crystal, indicating that it is likely an intrinsic property of the topaz. Luminescence of vicinal face C is a strong yellow (a very broad peak centered near 600 nm) and polarized parallel to the c axis. The B and B' vicinal faces display a much weaker yellow luminescence similar to that in C. Combined with the intrinsic
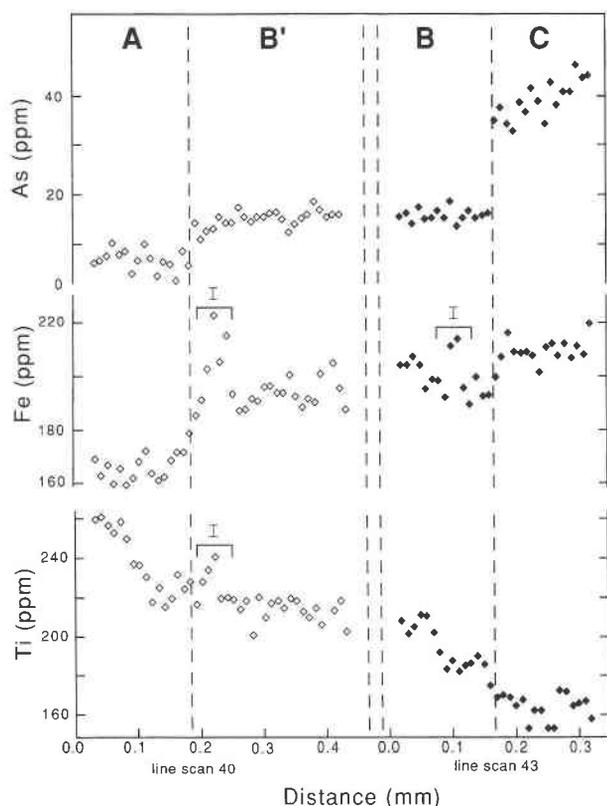
Fig. 4. SXRFMA data for As, Fe, and Ti are shown for two line scans. Line scan 40 traverses the subsectors beneath vicinal faces A and B', and 43 traverses from B into C (see Fig. 2). Dashed lines are subsector boundaries. Inclusions are marked I.

Fig. 5. Contour map of As concentration (ppm) from an SXRFMA area scan over the topaz (110) hillock shown in Fig. 2. Subsector A is below the 10-ppm contour, B and B' are generally within the contours of 10–20 ppm, and most of C is >40 ppm. An oxide inclusion somewhat obscures the A-B' subsector boundary.

this location. Hillock morphologies on {110} range from nearly square to elongate parallel to c and vary in vicinal face slope (from 0.1 to 1.0°) and degree of curvature of vicinal face A (from nearly straight to semicircular). This diversity likely results from slight differences in the crystallization environment (temperature, pressure, and fluid composition). All hillocks on all {110} faces of a given crystal possess identical morphologies. CL was also observed to vary slightly in intensity, but not in pattern. All samples analyzed by SXRFMA showed the same trends of trace element concentration, but absolute concentrations varied, as did the degree of partitioning between subsectors. For example, differences in As concentration between the subsectors C and A range from 2:1 to 9:1 in different crystals, but C is always the most enriched in As. None of the crystals were found to be completely unzoned. Similar zoning patterns were observed in several of the Utah samples.

Other forms

Three other forms display some degree of compositional zoning associated with spiral growth hillocks, but they are much less developed than {110}. Complete characterization of each is beyond the scope of this paper, but the observed CL and compositional differences are sim-
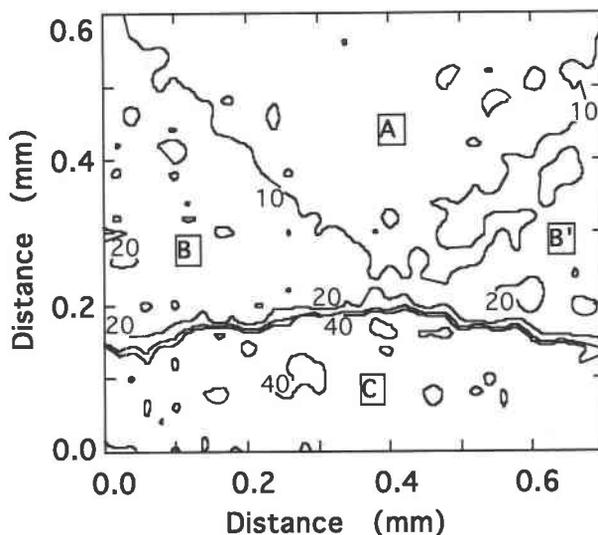
ilar to those for {110}. The {010} surfaces feature rectangular hillocks with straight growth steps parallel to [100] and [001]. Mirrors perpendicular to a and c relate opposing vicinal faces. Compositional differences between the two pairs of subsectors, designated E and F, were found to be nearly 8:1 for As (Fig. 6) and smaller, but significant, for Fe (1.4:1), Ti (1.2:1), and Ga (1.4:1). The (010) section analyzed showed a significant difference for Ga not seen in the {110} growth sector; Ge concentration showed no measurable differences. In contrast to observations on {110}, the vicinal faces with the steeper slope (F) are not enriched in Fe and As.

The {111} form displays hillocks with four nonequivalent vicinal faces. Steps are significantly curved on two adjacent vicinal faces. Observed differences in trace element concentrations among the four subsectors, R, S, T, and U, were small: 1.2:1 for Ti, 1.1:1 for Fe, and 1.3:1 for As (Fig. 7). Ga and Ge did not show significant differences in concentration within the (111) sector. In most cases, {001} faces featured only rounded hillocks. A few samples show six-sided polygonized hillocks. Four equivalent vicinal faces with growth steps parallel to ⟨110⟩ differ in CL character from two vicinal faces defined by steps parallel to ⟨010⟩.

CL of sections through several topaz crystals also indicated complex sectoral zoning. Sections 0.5–2 mm thick and bulk crystal sectors were examined by SXRFMA. Unfortunately, uncertainties of trace element concentrations determined in this manner are greater because of variations in sample thickness and superimposed intrasectoral zoning. Points were analyzed in time-equivalent growth zones (i.e., within a continuous concentric band)
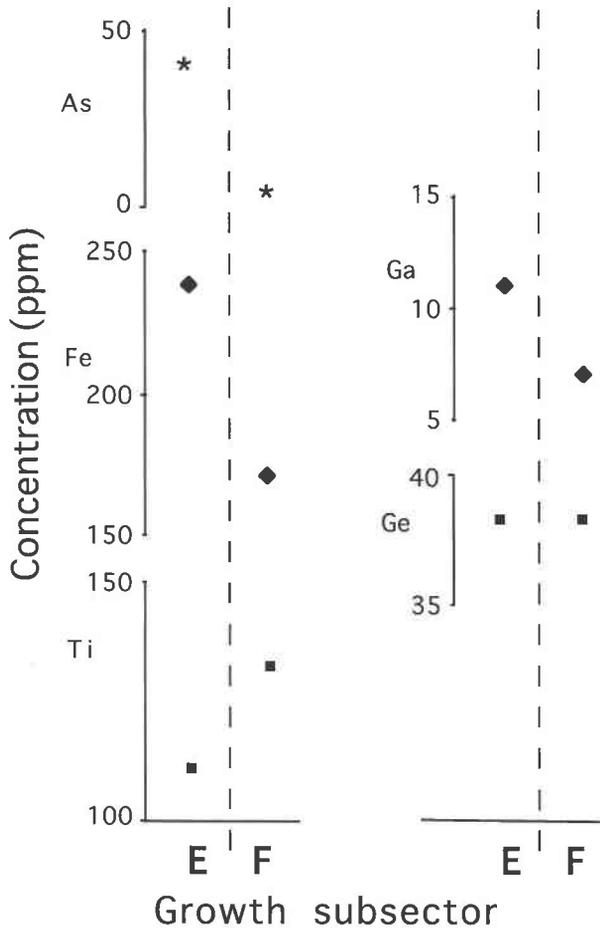
Fig. 6. SXRFMA point analyses of two nonequivalent subsectors within the (010) growth sector. Growth steps are parallel to [100] (on the corresponding vicinal face for subsector E), and parallel to [001] (for F). Precision is within the size of the symbols.

of several sectors (Table 2). Ti concentrations ranged from 76 ppm in the {110} sector to 295 ppm in {112}, Fe ranged from 134 ppm in {021} to 305 ppm in {101}, and As ranged from 5 ppm in {110} to 513 ppm in {112}. Differences in Ga and Ge may also be significant. In addition, Nb was found to be present in significant concentrations in only two sectors: 9 ppm in {010} and 46 ppm in {001}.

DISCUSSION

The observations reported here demonstrate that important differences exist in both the kinetic and the incorporation behavior of structurally distinct surfaces on topaz during crystal growth. Kinetic differences are expressed by the anisotropy in slope and step curvature of vicinal faces of the polygonized growth hillocks. Surface microtopography, cathodoluminescence, and trace element concentrations in time-equivalent regions are directly correlated, indicating that differential incorporation occurred during crystal growth. Sectoral and
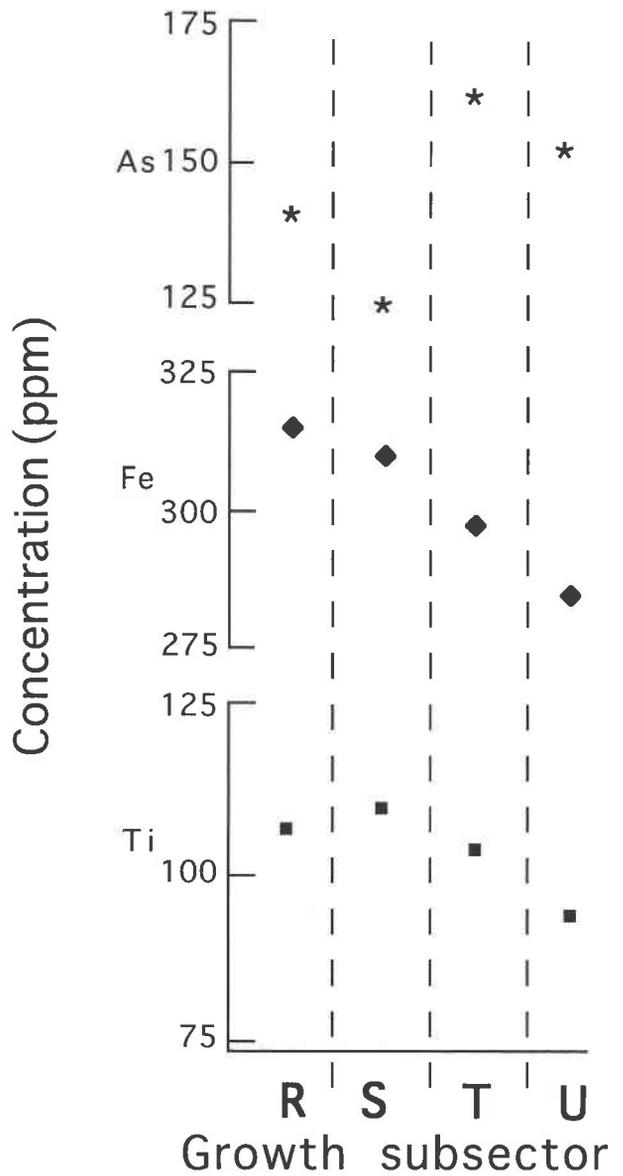

Fig. 7. SXRFMA point analyses of subsectors beneath four nonequivalent vicinal faces, R, S, T, and U, of a hillock on a (111) surface section. Ga and Ge do not vary significantly and are not shown. Precision is within the size of the symbols.

intrasectoral zoning patterns are seen to crosscut concentric zonation. Furthermore, the patterns strictly obey surface symmetry constraints. These observations, as discussed below, present substantial evidence that the detailed surface growth step structure exerts a strong, fundamental influence on both incorporation and growth.

All surfaces must have experienced essentially identical conditions during growth, so the observed effects result from structural differences of the surfaces themselves. It is possible that differences in fluid trace-element concentrations may be formed in the near-surface environment of the growing crystal, but such an effect would only be

TABLE 2. Average SXRFMA results for topaz crystal MX-200, showing sectoral zoning

Growth sector	{110}	{120}	{010}	{021}	{101}	{111}	{112}	{001}
Ti (ppm)	76(4)	110(5)	86(4)	114(5)	152(8)	169(8)	295(15)	199(10)
Fe (ppm)	189(8)	268(11)	171(7)	134(5)	305(12)	185(7)	166(6)	261(10)
Ga (ppm)	11(2)	11(2)	8(2)	8(2)	14(3)	12(2)	11(2)	14(3)
Ge (ppm)	35(3)	35(3)	33(3)	32(3)	27(3)	25(3)	25(3)	30(3)
As (ppm)	5(1)	14(1)	13(1)	56(1)	258(3)	124(1)	513(5)	129(2)
Nb (ppm)	2(3)	5(5)	9(3)	3(3)	2(3)	3(3)	3(3)	46(3)

Note: the {011} growth sector is not represented in this sample; however, by analogy to other samples analyzed, it would have the following approximate composition, relative to the above values: Ti, 90 ppm; Fe, 150; Ga, 9; Ge, 15; As, 20; and Nb, <3.

produced by differential incorporation. Any such local differences in the fluid composition would tend to oppose, rather than induce, the observed zoning patterns. Also, it seems unlikely that significant diffusion gradients are sustained during vapor-growth at high temperatures.

Differences in kinetic behavior of growth steps

The slope of a vicinal face is an expression of growth kinetics and reflects lateral growth rate (step-spreading rate), step height, and interstep spacing. Relative spreading rates of steps migrating in different directions determine growth hillock morphology, analogous to the control of crystal morphology by relative growth rates of faces. The vicinal face slope differs for each of the three nonequivalent step orientations on topaz {110}, indicating that lateral growth rate was not the same across the surface at a given time. Such differences must result from physical differences of the growth steps. Since incorporation of material occurs primarily at kink sites within growth steps, it follows that the properties of these kink sites are ultimately responsible for the differences in kinetic behavior.

The degree of curvature of the steps also varies systematically. Complementary to lateral growth rate, the curvature of growth steps reflects the tendency for steps to become aligned with directions of strong bonding in the structure. Step curvature represents an increased density of kink sites relative to that in straight step segments. Interestingly, the largest differences in both slope and curvature occur between vicinal faces A and C, both composed of growth steps nominally parallel to [001] but that advance in opposite directions. In addition, the degrees of hillock development and of step curvature differ on nonequivalent forms on a single crystal. These observations indicate that optimal growth conditions for the formation of perfectly polygonized hillocks vary with surface structure and are not the same for all forms present. In the topaz crystals examined, vicinal faces on {110}, {001}, {010}, and {111} are composed of 11 distinct growth-step orientations, each with its own particular kinetic characteristics. In all cases, on a given surface, symmetrically equivalent growth-step orientations behave similarly.

Strict adherence of such behavior to all face symmetry operators further indicates that kinetic and mechanistic properties are controlled by detailed surface structure and, to a reasonable first approximation, surface structure is

an expression of the internal crystal structure truncated by appropriate microtopography. Although some degree of surface reconstruction or relaxation may occur during growth and could influence kink-site geometry, our findings indicate that such processes do not affect the symmetry of hillocks or trace element incorporation patterns: all observations are consistent with face (plane group) symmetry. Reconstruction or relaxation processes themselves would be strongly influenced by the bulk crystal structure and symmetry.

Differences in incorporation of trace elements

Trace element compositional differences between subsectors that formed simultaneously on the topaz {110} surface are exactly correlated to the regions with presumed differences in kink-site structure described above. Furthermore, all surface regions that are constrained by surface symmetry to have equivalent kink-site structures (i.e., vicinal faces that are equivalent) are represented by subsectors possessing identical composition. In this regard, topaz and calcite show strong similarities. In calcite (Paquette and Reeder, 1990; Staudt et al., 1994), a correlation has been established between the detailed geometry and coordination of modeled kink sites and the relative affinities for specific trace elements. However, these specific site differences in topaz are not yet resolved.

It is important to note that the observed trace elements are each differentiated in a specific manner rather than all being enriched or depleted in any given subsector. With respect to intrasectoral zoning on {110} and {010}, Fe and As show differentiation opposite to Ti, whereas on {111}, Ti and Fe have similar distributions but opposite to that of As. Furthermore, not all elements show differential incorporation on all forms displaying intrasectoral zoning. Such chemical selectivity is additional evidence for significant differences in incorporation sites. Both the incorporation differences and the kinetic differences are apparently independent, primary effects due to surface structure. For example, there are no obvious correlations between vicinal face slope (or curvature) and trace element concentrations, either in bulk or individual elements.

As crystal faces advanced during growth, the microtopographically constrained incorporation patterns resulted in subsectors that are compositionally distinct. These can only have been formed during growth, as any later processes such as diffusion would destroy the intricate com-
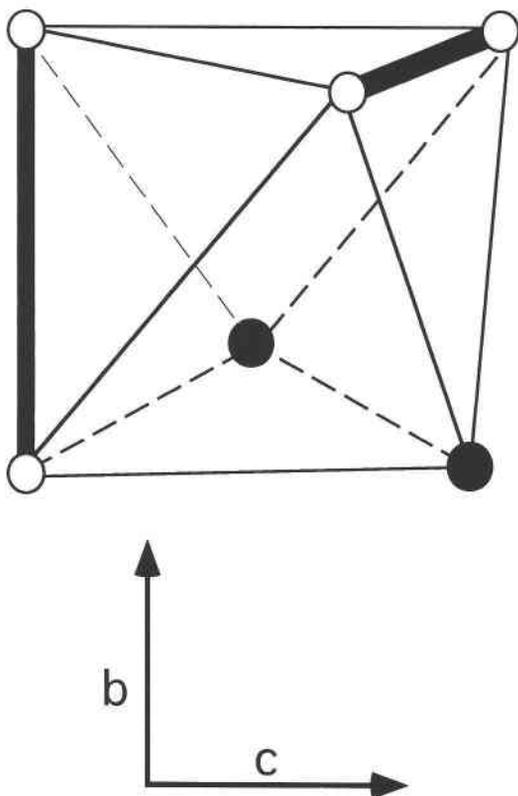
Fig. 8. The $^{[6]}$Al coordination polyhedron. Bold lines are O-O edges shared with adjacent octahedra; solid circles represent F atoms, and open circles are O atoms. Al in the center is not shown.

positional heterogeneities. Even at the relatively high temperatures during and immediately after formation, trace element diffusion in topaz does not appear to have affected the observed sharply defined zoning patterns. The uniformity of CL and of most trace element concentrations within subsectors indicates that trace elements are incorporated into crystallographic sites rather than concentrated in defects, inclusions, or a surface layer.

Surficial expressions of crystallographic sites

Topaz is orthorhombic, with space group *Pbnm*. Its structure (Alston and West, 1928; Pauling, 1928; Ribbe and Gibbs, 1971) consists of convoluted chains of edge-sharing $^{[6]}$Al polyhedra linked by isolated silicate tetrahedra, a configuration similar to the aluminosilicate polymorphs (kyanite, andalusite, and sillimanite), zoisite, and staurolite. A review of topaz structure and chemistry is given by Ribbe (1980). Because the topaz structure is based on a dense packing of anions and has little room for interstitial substitution, trace elements reported in these crystals probably substitute for Si or Al, although the specific sites have not been determined conclusively. On the basis of size consideration, Fe^{3+}, Ga^{3+}, and Mn^{3+}

are expected to replace $^{[6]}Al^{3+}$, and Ge^{4+} is expected to replace $^{[4]}Si^{4+}$. Ti^{4+} is too large for the Si tetrahedron and probably substitutes for $^{[6]}Al^{3+}$, with charge compensation by O^{2-} for F^-. Nb^{5+} is larger than Ti^{4+} and should also replace Al^{3+}, perhaps with a coupled substitution of $2O^{2-}$ for $2F^-$.

The structural location and valence state of As, which shows the largest differences in incorporation, are less predictable. Little work has been done on the substitution of As into silicates. As^{5+} may replace $^{[4]}Si^{4+}$, with charge balance accommodated on an adjacent $^{[6]}Al$ site. Substitution of As^{3+} for $^{[6]}Al^{3+}$ is also possible. Since As^{3+} has a lone pair of electrons, its presence in an octahedral site could play a role in CL activation. Yellow CL is most strongly correlated to As concentration, although As has not been previously reported as a CL activator, and other causes for luminescence are possible. CL-activation relationships in natural crystals are inherently complex. The observed luminescence in topaz has not been specifically investigated to our knowledge, nor have the activators responsible been identified.

At the growing surface, each crystallographic site can present different surface-site configurations, depending on the orientation of the surface, the orientation of growth steps, their detailed structure, and the location and orientation of the site. This is especially important for the Al octahedron. This coordination polyhedron (Fig. 8) consists of two adjacent F atoms and two O-O edges shared with neighboring octahedra. In the bulk structure, the Al-F distances (1.8 Å) are shorter than the Al-O distances (1.9 Å), and the shared O-O edges (2.5 Å) are shorter than the unshared edges (2.8 Å). The result is a highly distorted octahedron, which can present a variety of sites with different coordination and geometry exposed at the surface.

Such differences as are possible for Al surface sites should strongly influence trace element incorporation. Impurity ions may be directly discriminated by site geometry and coordination on the basis of size and charge. For elements requiring a coupled substitution for charge balance, incorporation may be greatest where both substitution sites are oriented favorably on the surface. In addition, ions that are present as fluoride complexes (as is common for As) or oxide complexes (as is common for Nb) may be differentiated on the basis of their fluid species. The orientation of the two F sites in the octahedral coordination polyhedron with respect to the exposed kink-site structure could have a profound effect on As incorporation. Careful modeling of surface configurations can be used to address the behavior of specific trace elements in light of the above processes.

The Si tetrahedron is much more symmetric, located on the mirror plane, and probably has a more limited variety of surficial expressions. Most likely as a result of this lack of surface-site diversity, the smallest extent of differential incorporation of the trace elements studied here involves Ge substitution for Si.

Geochemical implications

We have shown that distinct regions having nonequivalent surface structures differ in growth characteristics and in trace element incorporation, whereas regions with structures related by surface symmetry behave similarly in all respects. This work supports the conclusions drawn from calcite (Paquette and Reeder, 1990) that nonequivalent surficial expressions (such as kink sites within growth steps) of crystallographic sites that are equivalent in the bulk are responsible for the described effects. The effective D value for a trace element is then a function of crystal surface structure. Measured bulk-distribution coefficients for crystals formed from a given fluid composition under similar conditions may vary with crystal morphology, growth mechanism, growth hillock morphology, and crystal region sampled. With respect to sectoral zoning, bulk composition will be dominated by that of the dominant growth sector (the dominant crystal form). With regard to intrasectoral zoning resulting from spiral growth, the composition of a sector depends on the morphology and placement of surface growth hillocks, i.e., the relative dominance of vicinal faces. Geochemical investigations utilizing element distributions should therefore consider the arrangement of sectors and subsectors within a single crystal before drawing conclusions from a bulk D. As our ability to detect trace elements improves, closer examination reveals ever-greater complexity.

The concept of the nonequivalent surficial representation of crystallographic sites that are equivalent in the bulk also lends itself to ordering processes. Although the compositionally zoned samples used in this study have low OH content and show no evidence of ordering, it is important to address the relationship between differential incorporation and ordering. Ordering of OH and F in topaz is believed to be responsible for anomalous optical properties (Akizuki et al., 1979). In many OH-rich topaz crystals, optical properties differ sharply between nonequivalent growth sectors to produce an optical form of sectoral zoning. Parise et al. (1980), utilizing single-crystal neutron diffraction, verified OH and F ordering in optically anomalous growth sectors. Akizuki et al. (1979) concluded that specific planar surface orientations allow sites that are crystallographically equivalent to appear nonequivalent during growth, resulting in ordering in those sectors. A more detailed investigation of surface kink sites should relate this ordering mechanism to the processes responsible for differential incorporation.

This study documents a small part of the complexities of trace element incorporation in topaz, yet it has implications for trace element geochemistry in general. Preliminary examination of topaz from a wide variety of igneous, metamorphic, and hydrothermal regimes revealed at least some differential incorporation in nearly all samples. Intrasectoral zoning has also been observed in apatite (Rakovan and Reeder, 1994) and zoisite (Northrup and Rakovan, personal communication). Intrasectoral zoning can theoretically exist wherever symmetrically nonequivalent growth-step orientations are produced during crystal growth. It is usually associated with, but not limited to, growth by the spiral mechanism. It would not be surprising to find that differential incorporation resulting from surface-site selectivity is indeed commonplace.

REFERENCES CITED

Akizuki, M., Hampar, M.S., and Zussman, H. (1979) An explanation of anomalous optical properties of topaz. Mineralogical Magazine, 43, 237–241.

Alston, N.A., and West, J. (1928) The structure of topaz. Proceedings of the Royal Society A, 121, 358–367.

Criss, J.W. (1977) NRLXRF, a Fortran program for X-ray fluorescence analysis. Naval Research Laboratory, Washington, DC.

Dowty, E. (1976) Crystal structure and crystal growth: II. Sector zoning in minerals. American Mineralogist, 61, 460–469.

Frank, F.C., Lang, A.R., Evans, D.J.F., Rooney, M.L.T., Spear, P.M., and Welbourn, C.M. (1990) Orientation-dependent nitrogen incorporation on vicinals on synthetic diamond cube growth surfaces. Journal of Crystal Growth, 100, 354–376.

Hartman, P., and Perdok, W.G. (1955) On the relations between structure and morphology of crystals. Acta Crystallographica, 8, 49–52.

Lu, F.Q., Smith, J.V., Sutton, S.R., Rivers, M.L., and Davis, A.M. (1989) Synchrotron X-ray fluorescence analysis of rock-forming minerals. Chemical Geology, 75, 123–143.

Nakamura, Y. (1973) Origin of sector-zoning in igneous clinopyroxenes. American Mineralogist, 58, 986–990.

Northrup, P., and Reeder, R.J. (1992) Trace element incorporation in topaz: The role of surface structure during crystal growth. Geological Society of America Abstracts with Programs, A130.

Paquette, J., and Reeder, R.J. (1990) New type of compositional zoning in calcites: Insights into crystal-growth mechanisms. Geology, 18, 1244–1247.

Parise, J.B., Cuff, C., and Moore, F.H. (1980) A neutron diffraction study of topaz: Evidence for lower symmetry. Mineralogical Magazine, 43, 943–944.

Pauling, L. (1928) The crystal structure of topaz. Proceedings of the National Academy of Science, U.S.A., 14, 603–606.

Rakovan, J., and Reeder, R.J. (1994) Differential incorporation of trace elements and dissymmetrization in apatite: The role of surface structure during growth. American Mineralogist, 79, 892–903.

Reeder, R.J. (1991a) Surfaces make a difference. Nature, 353, 797–798.
——— (1991b) An overview of zoning in carbonate minerals. In Society of Economic Paleontologists and Mineralogists Short Course Notes, 25, 77–82.

Ribbe, P.H. (1980) Topaz. In Mineralogical Society of America Reviews in Mineralogy, 5, 215–230.

Ribbe, P.H., and Gibbs, G.V. (1971) The crystal structure of topaz and its relation to physical properties of topaz. American Mineralogist, 56, 24.

Roedder, E., and Stalder, H.A. (1988) "Pneumatolysis" and fluid-retention evidence for crystal growth from a vapor phase. In Fluid inclusions: Geological Society of India Memoirs, 11, 1–12.

Staudt, W.J., Reeder, R.J., and Schoonen, M.A.A. (1994) Surface structural controls on compositional zoning of SO_4^{-2} and SeO_4^{-2} in synthetic calcite single crystals. Geochimica et Cosmochimica Acta, 58, 2087–2098.